

## Enhancing Quantum Control by Improving Shaped-Pulse Generation


John P.S. Peterson<sup>1,\*</sup>, Roberto S. Sarthour,<sup>2</sup> and Raymond Laflamme<sup>1,3,4</sup>

<sup>1</sup>*Institute for Quantum Computing and Department of Physics and Astronomy, University of Waterloo, Waterloo, Ontario N2L 3G1, Canada*

<sup>2</sup>*Centro Brasileiro de Pesquisas Físicas, Rua Doutor Xavier Sigaud 150, Rio de Janeiro – RJ, 22290-180, Brazil*

<sup>3</sup>*Perimeter Institute for Theoretical Physics, 31 Caroline Street North, Waterloo, Ontario N2L 2Y5, Canada*

<sup>4</sup>*Canadian Institute for Advanced Research, Toronto, Ontario M5G 1Z8, Canada*

 (Received 12 September 2019; revised manuscript received 8 March 2020; accepted 23 April 2020; published 22 May 2020)

Most quantum processors requires pulse sequences for controlling quantum states. Here we present an alternative algorithm for computing an optimal pulse sequence so as to perform a specific task, being an implementation of a quantum gate or a quantum-state preparation. In our method, we reduce greatly the number of parameters to be fitted by using a limited number of functions as the modulations for the amplitude and phase of the radio-frequency pulses. Unlike other algorithms, ours uses some approximations to make it fast and scalable, and uses some efficient methods to obtain pulses that are robust to common types of experimental errors. We demonstrate the success of the proposed algorithm by performing several real experiments for 4-, 7-, and 12-quantum-bit systems using NMR. In addition, we show the efficiency of the algorithm, finding pulses for controlling with good fidelity the quantum states of spins in fictional square two-dimensional lattices containing 16, 36, and 100 qubits.

DOI: [10.1103/PhysRevApplied.13.054060](https://doi.org/10.1103/PhysRevApplied.13.054060)

### I. INTRODUCTION

Precise control of quantum systems is necessary for many important experimental implementations in the areas of quantum information and quantum computation. Furthermore, the control must be faster than the decoherence times, which is paramount for quantum computing [1–3]. In general, the theoretical plans demand that external operations—mainly electric and magnetic time-dependent fields—or internal interactions be turned on and off as quickly as possible. These processes are the ones used to execute quantum gates [1]. Although many of these operations can be achieved very rapidly, in practice, small deviations are likely to affect profoundly the experimental results, since many of these processes are required for simulating or executing a quantum protocol. In experiments where high accuracy is necessary, these implementation errors can significantly affect the final results. The method to obtain the optimal conditions for performing the quantum gates is to use numerical calculations that can account for the imperfections and delays in the experimental apparatuses. Furthermore, it is possible to use numerical simulations to find the optimal forms of the external excitations needed for controlling the quantum systems. Currently, in a modern NMR equipment, it is possible to implement magnetic radio-frequency (rf)

pulses with amplitude and phase modulations, which are used to construct the quantum gates and/or to perform quantum simulations. These radio-frequency pulses are, in general, developed to be robust to various types of errors, such as calibration errors, relaxation, and variations of the resonance frequency. One of the main algorithms used to obtain these modulated pulses is the gradient-ascent pulse engineering (GRAPE) algorithm [4]. GRAPE algorithms is being applied not only in NMR but also in many others experimental techniques and even in different areas [1,5–8]. In the NMR case, the optimization method consists in dividing the rf excitation into many small intervals of time, short pulses, and for each one fitting parameters (amplitude and phase) that will give the best description of the desired unitary operation. Other numerical methods of optimization were also implemented [9–17], attempting to ease the computational processes, which are hard due to the high number of parameters that must be taken into account. The number of parameters to be fitted is high because it is typically necessary to use tens of pulses, and sometimes hundreds. Constraints are also necessary, since it is hard for the NMR spectrometer to cope with rapid variations between the rf pulses, and thus smooth changes, from pulse to pulse, are required. This limits the search for the best parameters. These numerical calculations are, in general, very hard and take lots of computational time to be executed. In some cases, even after many computing hours, a satisfactory solution is not achieved. This is due mainly

\*johnpetersonps@hotmail.com

to the size of the system, the number of parameters, and equipment limitations. Although some progress has been made, there still a long way to go.

In this work, we present an algorithm to optimize external excitations that are used to manipulate the quantum states of relatively large systems. For this, only a reasonably small number of parameters to be optimized are necessary. Unlike other algorithms, ours uses some approximations to make it fast and scalable when it is used to optimize single-qubit rotations. In addition, the algorithm uses some efficient methods to obtain pulses that are robust to common types of experimental errors. Therefore, the time to perform the optimization is drastically reduced and we can obtain high-fidelity experimental results without other types of correction techniques (e.g., rf selection [18], rectification methods [19,20], and measurement-based feedback control [16]). We demonstrate the success of the proposed method by applying our algorithm in several real experiments, in which we manipulate the quantum states of NMR systems containing 4, 7, and 12 qubits. Furthermore, we show the efficiency of the algorithm, finding pulses for controlling with good precision the quantum state of spins distributed in fictional two-dimensional square lattices containing 16, 36, and 100 qubits. Finally, we discuss the application of our method in a larger system containing 65 536 qubits.

## II. OPTIMAL CONTROL THEORY

When we use a quantum system to perform a quantum computation or simulate the dynamics of other physical systems, generally we have to implement a unitary operator ( $U_{\text{goal}}$ ) that is not possible to produce only with the natural evolution of the system at hand. Hence, we need to add external interactions to modify the natural dynamics of the system. If we include these interactions, the total Hamiltonian of the system will be given by

$$\mathcal{H}_T(t) = \mathcal{H}_0 + \mathcal{H}_C(t), \quad (1)$$

where  $\mathcal{H}_0$  represents the natural Hamiltonian of the system and  $\mathcal{H}_C(t)$  is the control Hamiltonian, which describes the interactions used to modify the natural dynamics of the system.

The evolution of the system under the action of the Hamiltonian  $\mathcal{H}_T(t)$  will produce the following unitary operator:

$$U_{\mathcal{H}_T} = \mathcal{T} \left[ \exp \left( -\frac{i}{\hbar} \int \mathcal{H}_T(t) dt \right) \right]. \quad (2)$$

In Eq. (2),  $\mathcal{T}$  represents the Dyson time-ordering operator and  $\hbar$  is the Planck constant divided by  $2\pi$ . To have  $U_{\mathcal{H}_T} = U_{\text{goal}}$ , we must find the values of  $\mathcal{H}_T(t)$  that minimize the

function

$$\mathcal{F} = 1 - \frac{|\text{Tr}(U_{\text{goal}}^\dagger U_{\mathcal{H}_T})|}{N}, \quad (3)$$

where  $N$  is the dimension of the Hilbert space. The global minimum of  $\mathcal{F}$  can be very hard to find, since the number of operations needed in the control Hamiltonian, which are necessary to get  $U_{\mathcal{H}_T} = U_{\text{goal}}$ , is usually very high. However, using numerical optimizations, we can find local minima where  $U_{\mathcal{H}_T} \approx U_{\text{goal}}$ .

To perform a numerical optimization, the time must be discretized in  $m$  intervals of duration  $\delta t$ , which must be small enough to allow us to consider that  $\mathcal{H}_T(\delta t)$  is reasonably constant at each of the  $m$  intervals. In this case, we can calculate  $U_{\mathcal{H}_T}$  using the following equation:

$$U_{\mathcal{H}_T} = U_m U_{m-1} U_{m-2} \cdots U_2 U_1, \quad (4)$$

with

$$U_k = \exp \left( -\frac{i}{\hbar} [\mathcal{H}_0 + \mathcal{H}_C(k\delta t)] \delta t \right). \quad (5)$$

Many algorithms can be used to find local minima of  $\mathcal{F}$  [21]. The choice of one of these algorithms is usually based on the form of  $\mathcal{H}_T(t)$ . In our case,  $\mathcal{H}_T(t)$  will be the Hamiltonian of a system of nuclear spins that are controlled with use of the NMR technique.

## III. NMR

In the NMR technique, a sample containing many molecules, whose elements have nuclear spins, is placed in a uniform magnetic field along the  $z$  direction and radio-frequency pulses are used to control the quantum states of these spins. For a homonuclear NMR system, all the spins of interest have the same gyromagnetic ratio [22], since they are all of the same kind, and they are subjected to the same magnetic field along the  $z$  direction. However, because of the electrons clouds of the neighbor atoms, each individual nuclear spin is subjected to a slightly different magnetic field. This is known as chemical shift [22]. In addition, there is also the coupling interaction between the spins, which occurs via the exchange mechanism. Generally, the samples we use to simulate quantum systems or implement algorithms are isotropic liquids. The control of such systems is easier, since several interactions do not significantly influence the dynamics of these systems [22]. Thus, we consider samples that can be described by the following Hamiltonian:

$$\mathcal{H}_0 = \sum_k \frac{\hbar(\omega_k - \omega_R)\sigma_{z_k}}{2} + \sum_{k \neq n} \frac{\pi \hbar J_{kn} \sigma_{z_k} \sigma_{z_n}}{4}, \quad (6)$$

where  $\omega_k$  and  $\sigma_{\beta_k}$  are, respectively, the angular oscillation frequency and the Pauli matrix  $\beta$  of the  $k$ th nuclear spin,

$\omega_R$  is the angular frequency of the rotating frame, and  $J_{kn}$  is the scalar coupling constant of the spins  $k$  and  $n$ .

To control the quantum states of the nuclear spins, we use radio-frequency pulses applied in the  $x$ - $y$  plane with angular frequency  $\omega_R$ . The interactions of the spins with a pulse can be described by the following Hamiltonian:

$$\mathcal{H}_C(t) = \hbar\Omega(t) \sum_k \frac{\cos[\phi(t)]\sigma_{x_k} + \sin[\phi(t)]\sigma_{y_k}}{2}, \quad (7)$$

where  $\Omega(t)$  and  $\phi(t)$  represent the modulations of the pulse amplitude and its phase, respectively.

#### IV. THE ALGORITHM

According to Fermi's golden rule, time-dependent operations are necessary for inducing transitions between different energy levels. Experimentally, these transitions can be induced through the use of an oscillating electromagnetic field. In this way, electromagnetic fields can be used to implement quantum gates. The precise tailoring of these quantum gates is done through the modulation of the phase and amplitude of these fields. When the phase and amplitude do not have high symmetry, the optimal values for implementing a particular quantum gate must be found numerically. The current standard technique for finding these parameters is the GRAPE algorithm [4]. This algorithm optimizes the amplitude and phase at each time step, requiring hundreds of parameters for the construction of a quantum gate, which is a computationally arduous task. Furthermore, the GRAPE algorithm commonly requires many hours of computation and can, at times, result in gates with low fidelity [16]. The algorithm we propose in this work avoids processing large numbers of parameters by using a set of functions to find the shapes of the amplitude and the phase for the pulse. As a result, the number of parameters that need to be determined numerically is drastically reduced. For illustrative purposes, we present a formulation of our algorithm for finding pulses for the NMR technique. However, this algorithm can be extended to other techniques that use electromagnetic pulses for the control of a quantum system.

Since a Fourier series can be used to describe any function, we chose a limited series of sinusoidal functions where the amplitudes, frequencies, and phases have to be fitted. The functions produced by this fit will be the envelope of the amplitude and phase of the radio-frequency pulse. Thus, the amplitude and the phase of the pulse are modulated with use of sums composed of  $s_A$  and  $s_P$  sines, respectively:

$$\Omega(t) = \sum_{k=1}^{s_A} a_k \sin(b_k t + c_k), \quad (8)$$

$$\phi(t) = \sum_{k=1}^{s_P} d_k \sin(f_k t + g_k). \quad (9)$$

The variables  $a_k, b_k, c_k, d_k, f_k,$  and  $g_k$  must be optimized to obtain  $U_{\mathcal{H}_T} \approx U_{\text{goal}}$ . Generally, at the end of the optimization, the values of these variables will be of the same order as their initial value, remembering that an initial guess has to be given as an input. The values that the function  $\Omega(t)$  can assume must belong to the range  $[0, \text{Ap}]$ , where the upper bound will be established by the experimental equipment. To ensure that the function  $\Omega(t)$  does not exceed the lower bound, we have to shift this function so that its minimum is always positive. This can be accomplished with the following substitution:  $\Omega(t) \rightarrow \Omega(t) - \min \Omega(t)$ . Meanwhile, to limit the maximum value of  $\Omega(t)$ , we must find the maximum of this function,  $\Omega_{\text{max}} = \max \Omega(t)$ , and divide it by the limit of the amplitude,  $\Omega_{\text{max}}/\text{Ap}$ . If the result of this division is greater than 1, we need to make the following substitution:  $\Omega(t) \rightarrow \Omega(t)\text{Ap}/\Omega_{\text{max}}$ . The values of  $s_A$  and  $s_P$  will depend on the physical system (including limitations of the equipment used in the experiments), the type of unitary optimized, and the target fidelity of the optimized pulse. For rotations, we show in Sec. V D that  $s_A = 7$  and  $s_P = 14$  work well even with big systems. In our case, we consider  $s_P > s_A$  since our equipment is more accurate to generate the phase than the pulse amplitude.

We use a Nelder-Mead simplex algorithm to solve the optimization problem [21]. This algorithm does not use derivatives of the function  $\mathcal{F}$ . For the case where 63 parameters of Eqs. (8) and (9) ( $s_A = 7$  and  $s_P = 14$ ) are optimized, this algorithm converges faster than the optimization method used in GRAPE, which requires derivatives of  $\mathcal{F}$ .

When compared with GRAPE, another advantage of our method is that if we increase the pulse duration or reduce the interval  $\delta t$ , the number of variables that must be optimized does not increase. Consequently, the time to perform the optimization increases linearly. In our algorithm, we use this advantage to calculate  $U_k$  from Eq. (5) quickly. For this, we use the approximation presented in Ref. [23], which requires a small  $\delta t$  to calculate  $U_k$  with a high precision. Thus, for a system composed of  $q$  qubits, we have

$$U_k \approx e^{-i\phi(k\delta t)\Gamma} W_1 e^{-i\Omega(k\delta t)\Gamma\delta t} W_2 e^{i\phi(k\delta t)\Gamma}, \quad (10)$$

with  $\Gamma = \sum_{l=1}^q \sigma_{z_l}/2$ ,  $W_1 = e^{-i\mathcal{H}_0\delta t/2} H_q$ , and  $W_2 = H_q e^{-i\mathcal{H}_0\delta t/2}$ . The matrix  $H_q$  is the tensor product of  $q$  Hadamard gates.  $W_1$  and  $W_2$  need to be calculated only once. Since the other matrices of Eq. (10) are diagonal in the computational basis, to find  $U_{\mathcal{H}_T}$ , we need to calculate only exponentials of numbers and matrix products.

Although gradient-free optimization methods require more function evaluations, the union of our method with the approximation presented by Bhole and Jones [23] makes the average execution time of our algorithm less than that for GRAPE (with this approximation) for the systems presented in Sec. V.

Although this algorithm can be used to optimize gates of two qubits or more, we recommend the programmer decompose such gates into free evolutions under the Hamiltonian  $\mathcal{H}_0$  and gates of one qubit. By decomposing these gates, we can reduce the amount of errors, since pulse-calibration errors do not occur during free evolutions. Furthermore, the time for optimizing the pulse sequence that implements the quantum gates will also be shorter. Following this approach, the errors due to the free evolutions can be diminished with use of refocus sequences [24], the method presented by Ryan *et al.* [17], or an optimization method such as the one presented in Ref. [25].

### A. Considerations for the pulse amplitude

A common problem we have to consider is the initial and final values of the pulse amplitude. The rf generator and amplifiers have a limited time response that constrains the initial and final values of the pulse amplitude. This constraint can be solved if a smooth function  $\Omega(t)$  is used and it meets the following conditions:

- (a) The initial and final values of the amplitude must be null.
- (b) The rate of change of the amplitude, both at the beginning and at the end, has to be able to match the restriction due to the equipment used.

In our algorithm, we are able to satisfy these conditions by multiplying the function  $\Omega(t)$ , which describes the amplitude of a pulse with duration  $\tau_f$ , by the function

$$\Lambda(t) = -\tanh\left(\frac{\zeta_1 t}{\tau_f}\right) \tanh\left(\frac{\zeta_2(t - \tau_f)}{\tau_f}\right). \quad (11)$$

Then to correct the problems with the initial and final values of the amplitude, in Eq. (7) we have to perform the following replacement:  $\Omega(t) \rightarrow \Omega(t)\Lambda(t)$ . The rate of change of the amplitude may be reduced when  $\zeta_1$  and  $\zeta_2$  are reduced. These constants are determined experimentally. In general, when we reduce  $\zeta_1$  and  $\zeta_2$ , the optimization becomes more challenging. Because of this, we should look for the highest values of  $\zeta_1$  and  $\zeta_2$  that produce pulses that are well implemented. With our equipment we use  $\zeta_1 = \zeta_2 = 2$  and obtain good experimental results.

### B. Radio-frequency considerations

In our algorithm, we can also include a condition to obtain pulses that are robust to amplitude calibration. If we include this condition, we have to optimize two more unitary operations, which are given by

$$\begin{aligned} U_- &= \mathcal{T} \left[ \exp \left( -\frac{i}{\hbar} \int \mathcal{H}_0 + (1 - \varepsilon) \mathcal{H}_C(t) dt \right) \right], \\ U_+ &= \mathcal{T} \left[ \exp \left( -\frac{i}{\hbar} \int \mathcal{H}_0 + (1 + \varepsilon) \mathcal{H}_C(t) dt \right) \right]. \end{aligned} \quad (12)$$

The constant  $\varepsilon$  represents the value of the error in the calibration of the pulse amplitude. In our tests we use  $\varepsilon = 0.05$ , which is equivalent to an error of 5% in the pulse amplitude. The new function that we have to optimize will be given by the following weighted average:

$$\mathcal{F}_{\text{rf}} = \frac{\alpha_1 \mathcal{F}_- + \alpha_2 \mathcal{F} + \alpha_3 \mathcal{F}_+}{\alpha_1 + \alpha_2 + \alpha_3}, \quad (13)$$

where  $\alpha_1$ ,  $\alpha_2$ , and  $\alpha_3$  are the weights of each element of this average. The values of these weights are defined experimentally. Meanwhile, the values of  $\mathcal{F}_-$  and  $\mathcal{F}_+$  can be calculated by replacing  $U_{\mathcal{H}_T}$  by  $U_-$  and  $U_+$ , respectively, in Eq. (3).

In principle, because of the calculation of the new operators  $U_-$  and  $U_+$ , the number of operations we need to perform to obtain  $\mathcal{F}_{\text{rf}}$  is 3 times the number needed to obtain  $\mathcal{F}$ . However, with Eq. (10),  $\mathcal{F}_{\text{rf}}$  can be calculated efficiently, and the number of operations increases by approximately 50%. To achieve this improvement, during the calculation of  $U_-$ ,  $U_{\mathcal{H}_T}$ , and  $U_+$  we have to take into account that in Eq. (10) only the term that depends on  $\Omega(k\delta t)$  will change.

In modern NMR equipment, the errors in the amplitude calibration of the pulse are greater than the errors in the phase calibration [26]. Thus, we do not include conditions for the pulses to be robust to phase-calibration errors.

### C. Resonance frequency

As it was done for the error in the pulse amplitude, we can consider errors in the resonance frequency. In this case, to obtain the operators  $U_-$  and  $U_+$ , we must multiply  $\omega_k$  by  $(1 - \varepsilon)$  and  $(1 + \varepsilon)$ , respectively, instead of multiplying  $\mathcal{H}_C(t)$ . Therefore, if we use Eq. (10), only the matrices  $W_1$  and  $W_2$  will be modified in the calculation of  $U_-$  and  $U_+$ . In our experiments we do not include this condition, because the pulses obtained are already robust to this type of error. As an example, in a system with four qubits, we observe that even on our altering the frequency of resonance up to 30 Hz,  $\mathcal{F}$  remains less than 0.001.



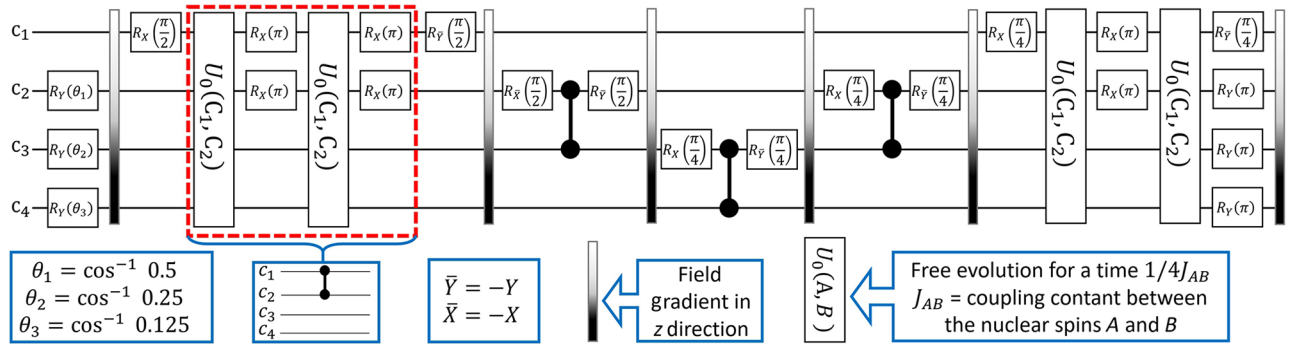


FIG. 1. Quantum circuit to prepare the pseudopure state  $|1111\rangle$  from a thermal state. In addition to rotations, we use free evolution and magnetic field gradients along the  $z$  direction. The field gradient is used to remove the nonzero coherence terms of the system state [27].

## V. EXPERIMENTAL RESULTS

For demonstration purposes, we perform some calculations using the algorithm and use these results in real NMR experiments. We present examples where the amplitude and the phase of the pulses are optimized so as to implement some quantum gates. The pulses are optimized from a random initial guess. In our tests, we optimize the pulses to implement sequences used to prepare the pseudopure state (PPS) [2] for a system with four and seven qubits, and some pulses to control a system of 12 qubits. After the numerical optimization, we perform the experiments using a Bruker Avance III 700-MHz NMR spectrometer. All experiments are performed at room temperature.

### A. Four-qubit system

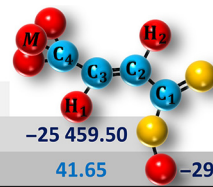
For these experiments, we use a sample of  $^{13}\text{C}$ -labeled *trans*-crotonic acid dissolved in acetone to implement the quantum circuit shown in Fig. 1. In theory, with this circuit we can prepare the pseudopure state  $|1111\rangle$  starting from a thermal state. In this molecule, the four  $^{13}\text{C}$  nuclear spins, under the action of a constant magnetic field, will physically represent a four-qubit system. The pulses are optimized by our considering that the H nuclear spins are decoupled; this can be achieved in the experiments. The resonance frequencies and the scalar coupling constants of the  $^{13}\text{C}$  nuclear spins that are used in our algorithm are shown in Fig. 2.

We optimize the phase and amplitude of the pulse to implement the rotations shown in the circuit in Fig. 1. The free evolutions are not optimized with our algorithm, since the  $\pi$  rotations and the magnetic field gradients correct most of the errors that occur during these evolutions. Each pulse lasts  $500 \mu\text{s}$ , and 63 parameters are optimized ( $s_A = 7$  and  $s_P = 14$ ) to obtain  $\mathcal{F}_{\text{rf}} < 0.0004$ , with  $\alpha_1 = \alpha_3 = 0.3$ ,  $\alpha_2 = 0.4$ , and  $\varepsilon = 0.05$ . In our simulations we notice that the number of parameters to be optimized can be reduced to 24 ( $s_A = 4$  and  $s_P = 4$ ), but in doing so we generally have to increase the duration of the

pulse. For the four-qubit system, we prefer to increase the number of parameters to reduce the duration of the pulse. When possible, we optimize the pulses to implement the largest number of simultaneous rotations. This reduces the total time of the experiment and, in general, increases the fidelity [3] of the results.

In Figs. 3(a) and 3(b), we graphically represent the amplitude and phase modulations of some of the pulses used to prepare the pseudopure state. We can see in Fig. 3(c) that even when we have errors in the calibration of the pulse amplitude, the rotation will still be implemented with high fidelity. This is due to the condition we add in our algorithm to find pulses that are robust to such errors.

After we implement the quantum circuit to prepare the pseudopure state, we determine the state of each qubit using the quantum-state-tomography method [28]. In Fig. 3(d), we present the fidelity between the states measured experimentally and the theoretical states. We also present in this same plot the fidelity between the states obtained by our simulating this circuit for the optimized pulses and the theoretical states. When we calculate the tensor product of the four-qubit state, which is determined experimentally, and compare with the theoretical prediction, we find a fidelity of 0.9993, which is exceptionally



$C_1$	-29 341.33			
$C_2$	72.27	-21 592.01		
$C_3$	1.17	69.67	-25 459.50	
$C_4$	7.04	1.45	41.65	-2989.19
	$C_1$	$C_2$	$C_3$	$C_4$

FIG. 2. Sample information for a  $^{13}\text{C}$ -labeled *trans*-crotonic acid molecule. The off-diagonal terms in the table are the  $J$  coupling constants of the  $^{13}\text{C}$  nuclear spins of the  $^{13}\text{C}$ -labeled *trans*-crotonic acid molecule. The chemical shifts of each nuclear spin are on the diagonal. The values are given in hertz.

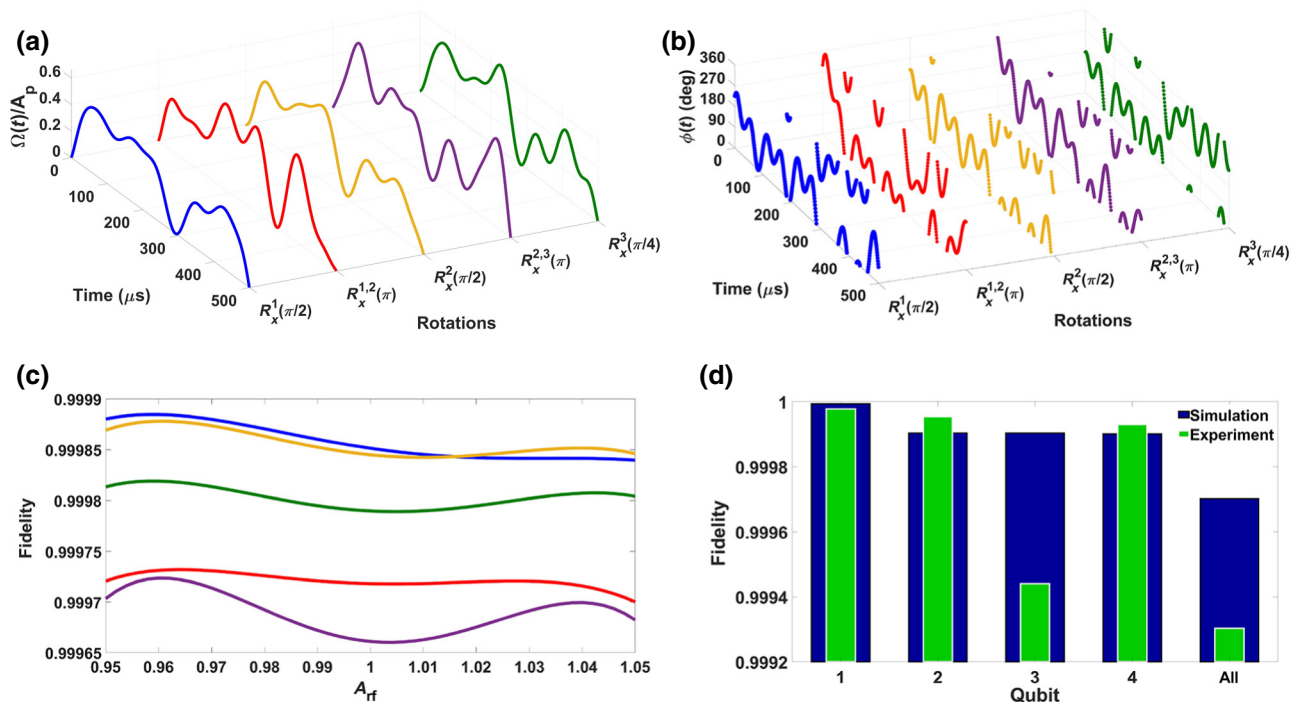


FIG. 3. Modulation of (a) the amplitude and (b) the phase of some pulses that are used to implement the rotations present in the quantum circuit shown in Fig. 1.  $R_{\Phi}^{a_1, \dots, a_n}(\theta)$  represents a rotation with angle  $\theta$  around the axis  $\Phi$  that is implemented in the state of the qubits  $a_1, \dots, a_n$ . The pulses are optimized to implement these rotations in the target qubits ( $a_1, \dots, a_n$ ) and to correct the evolution to leave the nontarget ones in their initial states. The pulses are seen to have very smooth shapes. (c) Rotation fidelity when we multiply the function that describes the pulse amplitude by  $A_{\text{rf}}$ . (d) Fidelity obtained in the simulation and experimental implementation of the quantum circuit used to prepare the pseudopure state  $|1111\rangle$ . To calculate the fidelity, we determine the experimental state of each qubit using the quantum-state-tomography method. The last point in the graph is obtained by the calculation of the tensor product of the four experimentally determined states.

good. To prove that we achieve high fidelity, we can compare our results with the results presented by Xin *et al.* [29]. They used the same molecule ( $^{13}\text{C}$ -labeled *trans*-crotonic acid) and the GRAPE algorithm to optimize the pulses. Their pseudopure-state fidelity was 0.9877. Because of our optimization method, we achieve better experimental results. All of our pulses have fidelity higher than 0.9996 and are well implemented. On the other hand, most of the one-qubit gates optimized by Xin *et al.* did not reach a fidelity of 0.9985.

## B. Seven-qubit system

We also run tests with a seven-qubit system. In this case, we use our algorithm to find the pulses that implement the rotations shown in the quantum circuit illustrated in Fig. 4. This quantum circuit is used to prepare the labeled pseudopure state  $|000000\rangle\langle 000000| \sigma_z/2$  [30], starting from a thermal state. The pulse optimization is performed by our considering that the nuclear spin of the hydrogen atoms of the per- $^{13}\text{C}$ -labeled (1S,4S,5S)-7,7-dichloro-6-oxo-2-thiabicyclo[3.2.0]heptane-4-carboxylic acid (Fig. 5) are decoupled. Thus, the nuclear spins of the  $^{13}\text{C}$  atoms

of this molecule will physically represent a seven-qubit system. Although it is possible to divide this seven-qubit system into subgroups to accelerate the pulse optimization [17], we do not use this strategy here since our objective is to verify if our algorithm can provide good results as the size of the system increases.

In our simulations we use the chemical shifts and the scalar couplings shown in Fig. 5. The amplitude and phase modulations of some of the pulses obtained with our algorithm are shown in Figs. 6(a) and 6(b).

Each pulse lasts 600  $\mu\text{s}$ , and 39 parameters are optimized ( $s_A = 5$  and  $s_P = 8$ ) to obtain  $\mathcal{F} < 0.004$ . When we simulate the quantum circuit shown in Fig. 4, using the pulses optimized with our algorithm, and compare the result with the theoretical state,  $|000000\rangle\langle 000000| \sigma_z/2$ , we find a fidelity greater than 0.99.

After the pulse optimization, we implement the quantum circuit to prepare the labeled PPS  $|000000\rangle\langle 000000| \sigma_z/2$  and determine the state of the nuclear spin that represents the seventh qubit. Theoretically, if the system is in this labeled PPS, when we implement a rotation of  $\pi/2$  in the state of the seventh qubit and measure its magnetization, we must obtain a spectrum with only one

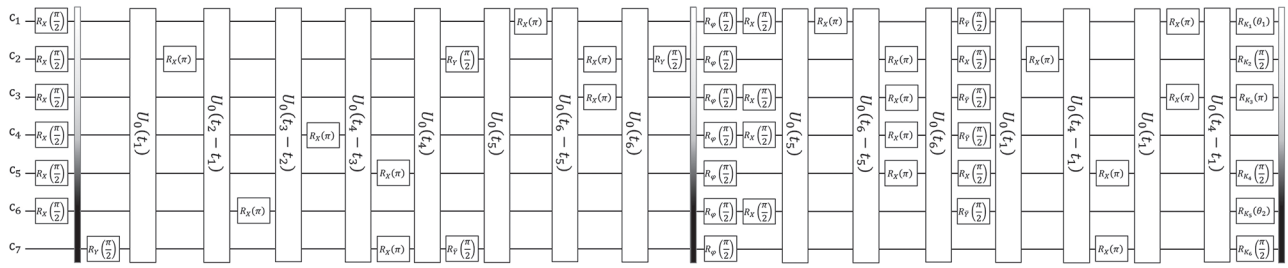


FIG. 4. Sequence to prepare the labeled pseudopure state  $|000000\rangle \langle 000000| \sigma_z/2$ .  $U_0(t_l)$  is a free evolution for time  $t_l$ , where  $t_1 = 1/4J_{C_2C_7}$ ,  $t_2 = 1/4J_{C_6C_7}$ ,  $t_3 = 1/4J_{C_4C_7}$ ,  $t_4 = 1/4J_{C_5C_7}$ ,  $t_5 = 1/4J_{C_1C_2}$ , and  $t_6 = 1/4J_{C_2C_3}$ .  $R_{K_l}(\theta_m)$  represents a rotation by angle  $\theta_m$  around an axis that belongs to the  $x$ - $y$  plane and forms an angle of  $K_l$  with the  $x$  axis. These angles are  $K_1 = 315^\circ$ ,  $K_2 = 67^\circ$ ,  $K_3 = 146^\circ$ ,  $K_4 = 92^\circ$ ,  $K_5 = 130^\circ$ ,  $K_6 = 26^\circ$ ,  $\theta_1 = 84^\circ$ , and  $\theta_2 = 110^\circ$ . This circuit needs to be implemented 7 times, and in the  $n$ th implementation we have  $\varphi = 2n\pi/7 + \pi/2$ . Finally, we sum the results of all experiments to get the labeled pseudopure state.

peak. In Fig. 6(c), we present the experimental spectrum obtained after implementation of the sequence to prepare the labeled PPS (followed by a  $\pi/2$  rotation in the state of the seventh qubit), along with the thermal-state spectrum. As the signal coming from the sample is weak compared with the noise, we perform 70 measurements to obtain the spectra. Even with this difficulty, we can see that it is possible to obtain a good experimental result with our algorithm to optimize the pulses. In this test we do not include the condition for the pulses to be robust to errors in their amplitude.

### C. 12-qubit system

Finally, we perform some experiments with a 12-qubit system. In this case, the nuclear spins of the five hydrogen atoms of the per- $^{13}\text{C}$ -labeled (1S,4S,5S)-7,7-dichloro-

6-oxo-2-thiabicyclo[3.2.0]heptane-4-carboxylic acid molecule (Fig. 5) are used to physically represent five qubits. The other seven qubits are represented by the carbon nuclear spins. To optimize the pulses, we divide this system into subsystems. If we do not follow this strategy, the optimization will be slow, since it would be performed in a Hilbert space of dimension  $2^{12}$ . In our case, we obtain good results with the following subsystems:  $\{C_1, C_2, C_3, H_4\}$ ,  $\{C_2, C_7\}$ ,  $\{C_3, H_2, H_3\}$ ,  $\{C_4, C_5, C_7, H_1\}$ , and  $\{C_5, C_6, C_7, H_5\}$ . The value of the function to be optimized,  $\mathcal{F}_{\text{sub}}$ , for a system composed of  $n$  subsystems is given by the following mean:

$$\mathcal{F}_{\text{sub}} = \frac{1}{n} \sum_k^n 1 - \frac{|\text{Tr}(U_{\text{goal}_k}^\dagger U_k)|}{N_k}, \quad (14)$$

C <sub>1</sub>	-30 020.09														
C <sub>2</sub>	57.58	-8780.39													
C <sub>3</sub>	-2.00	32.67	-6245.45												
C <sub>4</sub>	0.02	0.30	0.00	-10 333.53											
C <sub>5</sub>	1.43	2.62	-1.10	33.16	-15 745.40										
C <sub>6</sub>	5.54	-1.66	0.00	-3.53	33.16	-34 381.71									
C <sub>7</sub>	-1.43	37.43	0.94	29.02	21.75	34.57	-11 928.71								
H <sub>1</sub>	0.04	1.47	2.03	166.6	4.06	5.39	8.61	-3307.85							
H <sub>2</sub>	4.41	1.47	146.6	2.37	0.00	0.00	0.00	0.00	-2464.15						
H <sub>3</sub>	1.86	2.44	146.6	0.04	0.00	0.00	0.00	0.18	-12.41	-2155.59					
H <sub>4</sub>	-10.10	133.60	-6.97	6.23	0.00	5.39	3.80	-0.68	1.28	6.00	-2687.69				
H <sub>5</sub>	7.10	-4.86	3.14	8.14	2.36	8.52	148.5	8.46	-1.0	-0.36	1.30	-3645.08			
	C <sub>1</sub>	C <sub>2</sub>	C <sub>3</sub>	C <sub>4</sub>	C <sub>5</sub>	C <sub>6</sub>	C <sub>7</sub>	H <sub>1</sub>	H <sub>2</sub>	H <sub>3</sub>	H <sub>4</sub>	H <sub>5</sub>			

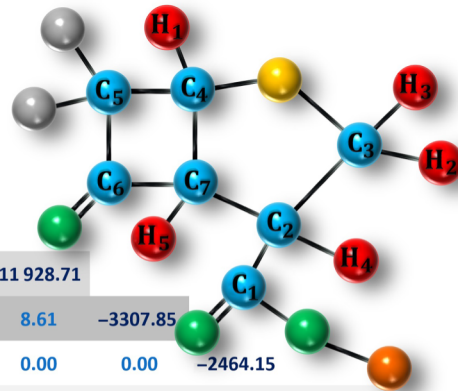


FIG. 5. Sample information for the per- $^{13}\text{C}$ -labeled (1S,4S,5S)-7,7-dichloro-6-oxo-2-thiabicyclo[3.2.0]heptane-4-carboxylic acid molecule. The off-diagonal terms in the table are the coupling constants  $J$  of the  $^{13}\text{C}$  and H nuclear spins of the per- $^{13}\text{C}$ -labeled (1S,4S,5S)-7,7-dichloro-6-oxo-2-thiabicyclo[3.2.0]heptane-4-carboxylic acid molecule. The chemical shifts of each nuclear spin are given on the diagonal. The values are given in hertz.

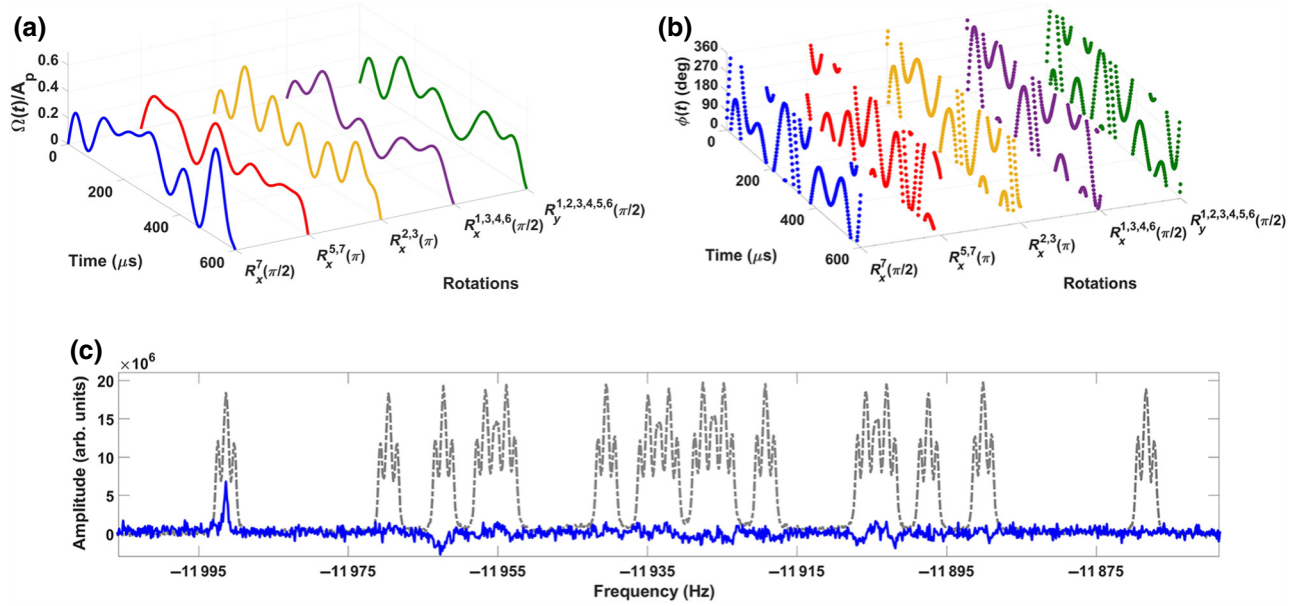


FIG. 6. Modulation of (a) the amplitude and (b) phase of some pulses that are used to implement the rotations present in the quantum circuit shown in Fig. 4.  $R_\Phi^{a_1, \dots, a_n}(\theta)$  represents a rotation by angle  $\theta$  around the axis  $\Phi$  that is implemented in the state of the qubits  $a_1, \dots, a_n$ . The pulses are optimized to implement these rotations in the target qubits ( $a_1, \dots, a_n$ ) and to correct the evolution to leave the nontarget ones in their initial states. (c) Thermal and labelled-PPS spectra of  $C_7$ . The blue line is the experimental spectrum obtained after the implementation of the sequence to prepare the labeled PPS followed by a  $\pi/2$  rotation in the seventh-qubit state. The dashed gray line is the experimental spectrum of the thermal state. To obtain the gray spectrum, we implement a rotation of  $\pi/2$  in the state of all nuclear spins and measure the system magnetization.

where  $U_k$ ,  $U_{\text{goal}_k}$ , and  $N_k$  represent, respectively, the optimized unitary operator, the goal unitary operator, and the dimension of the  $k$ th subsystem.

The signal coming from our sample is very weak when compared with the noise, and evaluating the results for some pulse sequences in this system can be very complicated. Because of this, we used only  $\pi/2$  rotations in our experimental tests. Thus, in the ideal case, the spectra of the nuclear spins that are targets of these rotations must contain peaks with maximum amplitude, and the spectra of the other spins will not show peaks. In addition, to analyze the experimental results, we can use the spectrum obtained by our applying a square fast pulse that implements a rotation of  $\pi/2$  in the state of all nuclear spins. This fast pulse has a duration of  $10 \mu\text{s}$  and its amplitude is calibrated to obtain a spectrum with maximum amplitude.

In Figs. 7(a) and 7(b), we present the shape of the amplitude and phase of two pulses that are optimized. The first pulse implements a rotation of  $\pi/2$  in the state of all nuclear spins. The second pulse implements a rotation of  $\pi/2$  in the nuclear spins of atoms  $C_1$ ,  $H_1$ , and  $H_5$ , which represent qubits 1, 8, and 12, respectively. Each pulse lasts 1 ms, and 78 parameters are optimized ( $s_A = 10$  and  $s_P = 16$ ) to obtain  $\mathcal{F}_{\text{sub}} < 0.007$ . One of the main difficulties to optimize the pulses is the fact that the resonance frequency of the nuclear spins of the hydrogen atoms differ by only a few hundred hertz. Because of this,

to individually control these spins, we have to increase the pulse duration and the number of parameters to be optimized.

After the optimization, we verify that the fidelity between the operator implemented by the optimized pulses ( $U_{\mathcal{H}_T}$ ) and the ideal operator ( $U_{\text{goal}}$ ) is greater than 0.97 by comparing the two matrices, the ideal matrix and the calculated matrix. To perform this calculation, we use Eqs. (4) and (5) for the complete system of 12 qubits to obtain  $U_{\mathcal{H}_T}$ . Because of the efficiency of our algorithm and because we use subgroups, when we perform simulate on the same computer a pulse with discretization of  $1 \mu\text{s}$ , the time required in the optimization to reach  $\mathcal{F}_{\text{sub}} < 0.007$  may be 25 times less than the time required to calculate  $U_{\mathcal{H}_T}$  of this pulse for the complete system of 12 qubits.

In Figs. 7(c) and 7(d), we present the spectra obtained experimentally after our implementing the optimized pulses along with the spectra obtained by our applying a fast square pulse. We can see from Figs. 7(c) and 7(d) that we achieve good experimental results, even without including in the optimization conditions the requirement for the pulses to be robust to some types of errors. In our tests, we verify that if we double the number of parameters to be optimized, it is possible to achieve a fidelity greater than 0.995 in the simulation. However, the experimental results will not be very different from those shown



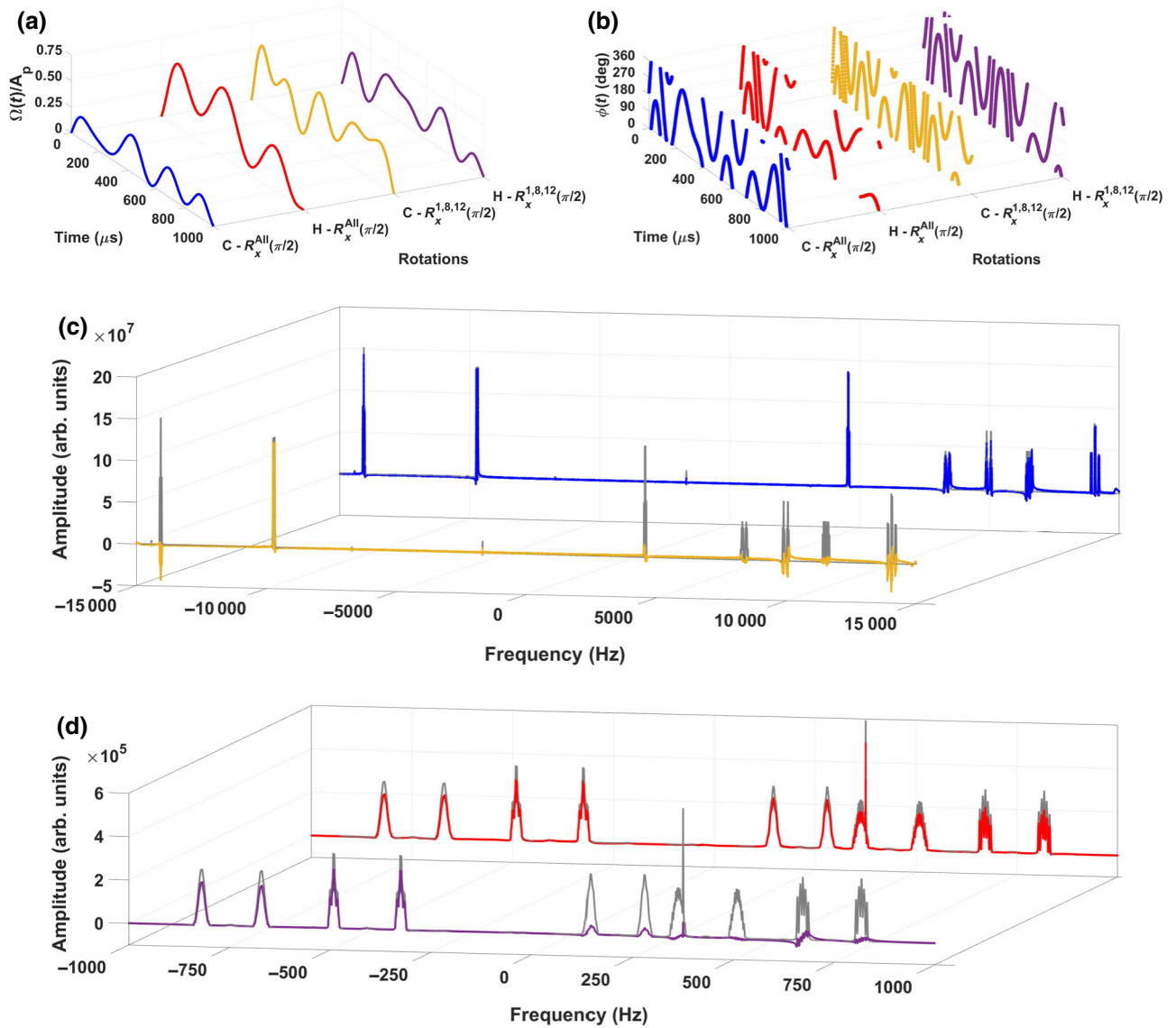


FIG. 7. Modulation of (a) the amplitude and (b) the phase of the pulses that are implemented in the 12-qubit system. As the hydrogen spins are very close in frequency, we use different shapes for the pulses applied with the hydrogen and carbon frequencies. This gives more freedom for the pulse optimization, and the target fidelity can be achieved quickly. “C” and “H” indicate that the pulses are applied simultaneously with a frequency close to the carbon resonance frequency and the hydrogen resonance frequency, respectively.  $R_{\Phi}^{a_1, \dots, a_n}(\theta)$  represents a rotation by angle  $\theta$  around the axis  $\Phi$  that is implemented in the state of the qubits  $a_1, \dots, a_n$  and to correct the evolution to leave the nontargets one in their initial states. Qubits 1 to 7 are represented physically by atoms  $C_1$  to  $C_7$  and qubits 8 to 12 are represented physically by atoms  $H_1$  to  $H_5$  of the per- $^{13}\text{C}$ -labeled (1S,4S,5S)-7,7-dichloro-6-oxo-2-thiabicyclo[3.2.0]heptane-4-carboxylic acid molecule. The pulses are seen to have very smooth shapes. (c) Carbon spectrum and (d) hydrogen spectrum. The gray line is the thermal spectrum obtained by our applying a fast square pulse that implements a rotation of  $\pi/2$  in the state of all qubits. The other spectra are obtained by our implementing the optimized pulses in (a),(b) and measuring the magnetization of the system in the rotating frame.

in Figs. 7(c) and 7(d). In this system, even delays of a few hundred nanoseconds can affect the final result. Therefore, if we want better experimental results in this system, we must include this and other sources of errors in our optimization. For the carbon nuclear spins, Fig. 7(c), we have to perform 128 measurements to increase the signal-to-noise ratio. Thus, during these measurements

(approximately 4 h) the variations of temperature and magnetic field are two other sources of errors that cannot be disregarded.

#### D. Simulations for 16, 36, 100, and 65 536 qubits

The performance of our algorithm may be impaired if we increase the number of parameters to be optimized,

since it is based on a Nelder-Mead simplex algorithm [21,31,32]. Therefore, we perform a test to verify if it is possible to optimize pulses quickly for larger systems for the same 63 parameters ( $s_A = 7$  and  $s_P = 14$ ) as used with the four-qubit system. The systems considered are two two-dimensional lattices with coupling between the nearest neighbors. Similar systems are already an experimental reality [33]. It is our belief that the algorithm described in our work can be useful for controlling them.

The lattices have 16 and 36 nuclear spins, which represent systems containing 16 and 36 qubits, respectively; see Fig. 8. These systems are controlled with the NMR technique. Thus, the natural Hamiltonian of the system will be  $\mathcal{H}_0$ , Eq. (6). The scalar coupling constant ( $J_{kn}$ ) between the nearest neighbors is 50 Hz. The angular oscillation frequency of the  $k$ th nuclear spin is given by  $\omega_k = 2\pi[b + s(k - 1)]$ , with  $b = 700$  MHz and  $s = 2$  kHz. The angular frequency of the rotating reference frame ( $\omega_R$ ) is equal to the mean of the angular oscillation frequencies of the first and last spins of the lattice.

In our test, we optimize the phase and amplitude of a pulse of 1 ms to implement a rotation of  $\pi/2$  on all the odd qubits of the lattice. As in the case of 12 qubits, here we perform the optimization in subsystems. The 16-qubit system is divided into seven groups of four qubits and the 36-qubit system is divided into 13 groups of four qubits and eight groups of two qubits, as shown in Fig. 8. In the optimization of the pulse in the 16-qubit system, it is possible to obtain  $\mathcal{F}_{\text{sub}} < 0.01$  in less than 1 h. In the 36-qubit system, after 1 h of optimization, we are able to obtain  $\mathcal{F}_{\text{sub}} < 0.025$ . The shapes of the amplitude and the phase of these pulses are shown in Fig. 9. To reduce the errors due to the approximation shown in Eq. (10), we decrease the pulse discretization during the optimization. Initially, we started with discretization  $\delta t = 5 \mu\text{s}$ , and we finish the optimization with  $\delta t = 0.625 \mu\text{s}$ .

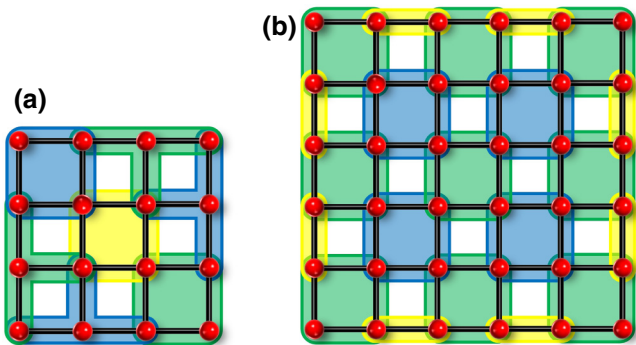


FIG. 8. Square two-dimensional lattice composed of (a) 16 qubits and (b) 36 qubits. Black bars indicate which nuclear-spin pairs have nonzero scalar coupling. The subgroups used in the optimization are shown in blue, green, and yellow.

In principle, the two main difficulties to optimize pulses to control large quantum systems are the time and the amount of memory needed to perform the simulation. If we divide these systems into subgroups, we can work around those problems. For example, we perform a test with a two-dimensional square lattice of size  $256 \times 256$ , which represents a system of 65 536 qubits. The amount of memory used in the optimization process is less than 2 GB, and the time to calculate all the quantities needed to obtain  $\mathcal{F}_{\text{sub}}$ , Eq. (14), is approximately 1 min (for a pulse of 1 ms and  $\delta t = 10 \mu\text{s}$ ). In our simulations, we use a computer with an Intel Core i7-8700 processor and 16 GB of RAM. The subgroups are divided following the same pattern used for the 36-qubit system (Fig. 8). While it is possible to work with such large systems with our algorithm, when we increase the size of the lattice without changing the number of optimized parameters, the maximum amplitude of the pulse, or duration of the pulse, we may have difficulty obtaining  $\mathcal{F}_{\text{sub}} < 0.01$  in the optimization of the pulses. This happens because the distance between the resonance frequency of the first and last spins of the lattice also increases. It is worth remembering that the error of the approximation presented in Eq. (10) will also increase when this distance increases. One way to solve this problem is to consider that the lattice is formed by more than one kind of atom and that we can use multiple rotating frames [2]. In this case, the resonance frequency of the atoms of a species may be several hundred megahertz different from the frequency of the atoms of the other species. When the difference between the pulse frequency and the resonance frequency of the nuclear spin increases, it will be more difficult for this pulse to change the state of the spin.

In our simulation we consider a spectrometer with five channels (five rotating frames), as used in Ref. [34]. As was done previously, we use 63 parameters ( $s_A = 7$  and  $s_P = 14$ ) to optimize the amplitude and phase of a pulse of 1 ms to implement a rotation of  $\pi/2$  on all the odd qubits of the lattice. In this case, the pulses applied in the five channels will have the same shape for the amplitude and phase but their oscillation frequencies will be different. We perform the simulation assuming the lattice is composed of 100 qubits. The lattice is composed of nuclear spins of  $^1\text{H}$ ,  $^{19}\text{F}$ ,  $^{13}\text{C}$ ,  $^{31}\text{P}$ , and  $^{15}\text{N}$  atoms. The lattice is configured to have the first 20 qubits represented by nuclear spins of  $^1\text{H}$ , the next 20 by nuclear spins of  $^{19}\text{F}$ , and so on. In each group of 20 spins, the resonance frequency of the  $k$ th nuclear spin of the group will be given by  $\omega_k^n = 2\pi[b_n + s(k - 1)]$ , where  $s = 2$  kHz and  $b_n$  represents the characteristic resonance frequency of the nuclear spin of the  $n$ th species of an atom of the lattice. If we consider NMR equipment with a magnetic field magnitude of 16.44 T, we have  $b_{\text{H}} = 700$  MHz,  $b_{\text{F}} = 658$  MHz,  $b_{\text{C}} = 176$  MHz,  $b_{\text{P}} = 283$  MHz, and  $b_{\text{N}} = -71$  MHz. To perform the optimization, we divide the system following

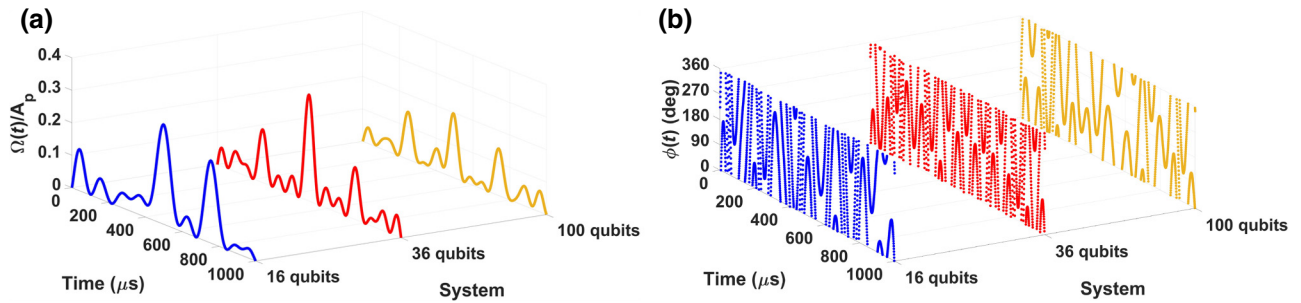


FIG. 9. Modulation of (a) the amplitude and (b) the phase of the pulses that are optimized to implement a  $\pi/2$  rotation on all odd spins of the lattice. Even for big systems, we can see that the pulses have very smooth shapes.

the same pattern used for the 36-qubit system (Fig. 8). After approximately 3 h of optimization, it is possible to obtain  $\mathcal{F}_{\text{sub}} < 0.012$ , with  $\delta t = 0.625 \mu\text{s}$ , which is an excellent result. The shape of the amplitude and the phase of the optimized pulse is illustrated in Fig. 9. It is worth remembering that this pulse is optimized with the same restrictions as used in the optimization of the pulses for a system of 7 and 12 qubits for it to be well implemented experimentally. It is possible to conclude from the results that even with a small number of parameters, our algorithm can efficiently optimize pulses for the big systems considered here. Since our algorithm can be fast and does not require a large amount of memory, we believe that it can contribute significantly to the control of large quantum systems that could be used as quantum computers, not only in NMR systems but also in other technologies.

## VI. CONCLUSIONS

In summary, we develop an algorithm for optimizing radio-frequency pulses, which are generally used in NMR systems to implement quantum gates with high fidelity. The pulses can be optimized to be robust to calibration errors and other types of errors. Besides, with our algorithm we can obtain pulses that have smooth modulations, since these pulses are described by a set of smooth functions. This is a good advantage over some other methods, since most NMR spectrometers do not deal well with fast variations of the pulse parameters. These functions can be chosen experimentally to ensure that the optimized pulses are implemented with high precision. Unlike other algorithms, ours uses a small number of parameters, approximations, and efficient methods to obtain pulses robust to common types of experimental errors. Because of this, our algorithm is fast, is scalable, and gives good experimental results if it is used to optimize rotations. We show the success of our algorithm using real NMR experiments, where systems composed of 4 to 12 qubits are controlled. Finally, we prove that even in a system with 100 qubits, the pulses used to implement rotations can be described by a small

number of parameters, and our algorithm can be efficient enough to optimize a modulated pulse in a short period. Because of the effectiveness of our optimization algorithm, we are able to obtain good experimental results without using any other error-correction technique (e.g., rf selection [18], rectification methods [19,20], and measurement-based feedback control [16]) or external calibration devices. Because of the effectiveness and efficiency of our algorithm, we believe that it can be used to control large quantum systems in other experimental techniques, other than NMR techniques. A future challenge will be to use this algorithm to control systems containing thousands of qubits.

## ACKNOWLEDGMENTS

We thank Hemant Katiyar and Janet Venne for valuable discussions that helped to develop the ideas presented in this paper. We thank Shayan-Shawn Majidy for valuable comments on the manuscript. We acknowledge financial support from the Ministry of Innovation, Science and Economic Development (Canada), the Government of Ontario, CIFAR, Mike and Ophelia Lazaridis, CNPq, and FAPERJ.

- 
- [1] S. J. Glaser, U. Boscain, T. Calarco, C. P. Koch, W. Köckenberger, R. Kosloff, I. Kuprov, B. Luy, S. Schirmer, T. Schulte-Herbrüggen, D. Sugny, and F. K. Wilhelm, Training Schrödinger's cat: Quantum optimal control, *Eur. Phys. J. D* **69**, 279 (2015).
  - [2] I. Oliveira, R. S. Sarthour, T. Bonagamba, E. Azevedo, and J. C. C. Freitas, *NMR Quantum Information Processing* (Elsevier, Amsterdam, 2007).
  - [3] M. A. Nielsen and I. L. Chuang, *Quantum Computation and Quantum Information* (Cambridge University Press, Cambridge, 2000).
  - [4] N. Khaneja, T. Reiss, C. Kehlet, T. Schulte-Herbrüggen, and S. J. Glaser, Optimal control of coupled spin dynamics: Design of NMR pulse sequences by gradient ascent algorithms, *J. Magn. Reson.* **172**, 296 (2005).

- [5] Y. Zhang, C. A. Ryan, R. Laflamme, and J. Baugh, Coherent Control of Two Nuclear Spins Using the Anisotropic Hyperfine Interaction, *Phys. Rev. Lett.* **107**, 170503 (2011).
- [6] F. Dolde, V. Bergholm, Y. Wang, I. Jakobi, B. Naydenov, S. Pezzagna, J. Meijer, F. Jelezko, P. Neumann, T. Schulte-Herbrüggen, J. Biamonte, and J. Wrachtrup, High-fidelity spin entanglement using optimal control, *Nat. Commun.* **5**, 3371 (2014).
- [7] V. Nebendahl, H. Häffner, and C. F. Roos, Optimal control of entangling operations for trapped-ion quantum computing, *Phys. Rev. A* **79**, 012312 (2009).
- [8] R. Fisher, F. Helmer, S. J. Glaser, F. Marquardt, and T. Schulte-Herbrüggen, Optimal control of circuit quantum electrodynamics in one and two dimensions, *Phys. Rev. B* **81**, 085328 (2010).
- [9] D. Lucarelli, Quantum optimal control via gradient ascent in function space and the time-bandwidth quantum speed limit, *Phys. Rev. A* **97**, 062346 (2018).
- [10] T. E. Skinner and N. I. Gershenzon, Optimal control design of pulse shapes as analytic functions, *J. Magn. Reson.* **204**, 248 (2010).
- [11] I. I. Maximov, Z. Tošner, and N. C. Nielsen, Optimal control design of NMR and dynamic nuclear polarization experiments using monotonically convergent algorithms, *J. Chem. Phys.* **128**, 184505 (2008).
- [12] S. C. Hou, L. C. Wang, and X. X. Yi, Realization of quantum gates by Lyapunov control, *Phys. Lett. A* **378**, 699 (2014).
- [13] T. Caneva, T. Calarco, and S. Montangero, Chopped random-basis quantum optimization, *Phys. Rev. A* **84**, 022326 (2011).
- [14] P. Doria, T. Calarco, and S. Montangero, Optimal Control Technique for Many-Body Quantum Dynamics, *Phys. Rev. Lett.* **106**, 190501 (2011).
- [15] S. Machnes, E. Assémat, D. Tannor, and F. K. Wilhelm, Tunable, Flexible, and Efficient Optimization of Control Pulses for Practical Qubits, *Phys. Rev. Lett.* **120**, 150401 (2018).
- [16] D. Lu, K. Li, J. Li, H. Katiyar, A. J. Park, G. Feng, T. Xin, H. Li, G. Long, A. Brodutch, J. Baugh, B. Zeng, and R. Laflamme, Enhancing quantum control by bootstrapping a quantum processor of 12 qubits, *npj Quantum Inf.* **3**, 45 (2017).
- [17] C. A. Ryan, C. Negrevergne, M. Laforest, E. Knill, and R. Laflamme, Liquid-state nuclear magnetic resonance as a testbed for developing quantum control methods, *Phys. Rev. A* **78**, 012328 (2008).
- [18] C. A. Ryan, M. Laforest, and R. Laflamme, Randomized benchmarking of single- and multi-qubit control in liquid-state NMR quantum information processing, *New J. Phys.* **11**, 013034 (2009).
- [19] Y. S. Weinstein, T. F. Havel, J. Emerson, N. Boulant, M. Saraceno, S. Lloyd, and D. G. Cory, Quantum process tomography of the quantum Fourier transform, *J. Chem. Phys.* **121**, 6117 (2004).
- [20] O. Moussa, M. P. da Silva, C. A. Ryan, and R. Laflamme, Practical Experimental Certification of Computational Quantum Gates Using a Twirling Procedure, *Phys. Rev. Lett.* **109**, 070504 (2012).
- [21] Jorge Nocedal and S. Wright, *Numerical Optimization* (Springer-Verlag, New York, 2006), 2nd ed.
- [22] M. H. Levitt, *Spin Dynamics* (Wiley, Chichester, 2001).
- [23] G. Bhole and J. A. Jones, Practical pulse engineering: Gradient ascent without matrix exponentiation, *Front. Phys.* **13**, 130312 (2018).
- [24] J. A. Jones and E. Knill, Efficient refocusing of one-spin and two-spin interactions for NMR quantum computation, *J. Magn. Reson.* **141**, 322 (1999).
- [25] J. P. S. Peterson, R. S. Sarthour, A. M. Souza, I. S. Oliveira, F. Brito, and F. de Melo, Reliability of digitized quantum annealing and the decay of entanglement, *Ann. Phys.* **530**, 1800007 (2018).
- [26] Bruker BioSpin, *Pulse Programming*, Manual for TopSpin 2.1 Version 2.1.1 (Bruker BioSpin GmbH, Rheinstetten, 2008).
- [27] P. Nicholas, D. Fushman, V. Ruchinsky, and D. Cowburn, The virtual NMR spectrometer: A computer program for efficient simulation of NMR experiments involving pulsed field gradients, *J. Magn. Reson.* **145**, 262 (2000).
- [28] G. M. Leskowitz and L. J. Mueller, State interrogation in nuclear magnetic resonance quantum-information processing, *Phys. Rev. A* **69**, 052302 (2004).
- [29] T. Xin, S. Huang, S. Lu, K. Li, Z. Luo, Z. Yin, J. Li, D. Lu, G. Long, and B. Zeng, NMRcloudQ: A quantum cloud experience on a nuclear magnetic resonance quantum computer, *Sci. Bull.* **63**, 17 (2018).
- [30] A. J. Park, E. McKay, D. Lu, and R. Laflamme, Simulation of anyonic statistics and its topological path independence using a seven-qubit quantum simulator, *New J. Phys.* **18**, 043043 (2016).
- [31] J. C. Lagarias, J. A. Reeds, M. H. Wright, and P. E. Wright, Convergence properties of the nelder-mead simplex method in low dimensions, *SIAM J. Optim.* **9**, 112 (1998).
- [32] L. Han and M. Neumann, Effect of dimensionality on the Nelder–Mead simplex method, *Optim. Methods Softw.* **21**, 1 (2006).
- [33] D. O. de Mello, D. Schäffner, J. Werkmann, T. Preuschoff, L. Kohfahl, M. Schlosser, and G. Birkel, Defect-Free Assembly of 2D Clusters of more than 100 Single-Atom Quantum Systems, *Phys. Rev. Lett.* **122**, 203601 (2019).
- [34] I. A. Silva, A. M. Souza, T. R. Bromley, M. Cianciaruso, R. Marx, R. S. Sarthour, I. S. Oliveira, R. Lo Franco, S. J. Glaser, E. R. deAzevedo, D. O. Soares-Pinto, and G. Adesso, Observation of Time-Invariant Coherence in a Nuclear Magnetic Resonance Quantum Simulator, *Phys. Rev. Lett.* **117**, 160402 (2016).